Available online at www.sciencedirect.com
SCIENCE DIRECT®
Journal of Solid State Chemistry 177 (2004) 2691–2698
JOURNAL OF SOLID STATE CHEMISTRY
http://elsevier.com/locate/jssc

Intercalation of noble metal complexes in LDH compounds

P. Beaudot, M.E. De Roy,* and J.P. Besse

Laboratoire des Matériaux Inorganiques, Université Blaise Pascal, UMR CNRS 6002, 63177 Aubière Cedex, France

Received 3 December 2003; received in revised form 24 March 2004; accepted 29 March 2004

Abstract

Intercalation of iridium, platinum, and ruthenium complexes was carried out in [ZnAl], [MgAl], and [CuAl] LDHs structures by a new method of hydrothermal synthesis. Carbonate-free products were obtained. XRD, FTIR and EXAFS studies confirmed total anion exchange for Ir and Pt containing compounds. However, the geometry of local environment of iridium or platinum atom in the complexes appeared modified during intercalation. By thermal treatments metallic particles dispersed on oxide powder were obtained.

Keywords: LDH; Intercalation; Iridium and platinum complexes; Dispersed metallic particles

1. Introduction

LDHs are a family of lamellar solids of the general formula $[M^{II}_{(1-x)}M^{III}_{(x)}(OH)_2]^{x+}[X^{m-}_{x/m}\cdot nH_2O]^{x-}$, where M is a metal cation and X is an interlayer anion. Their structure can be described as brucite-like layers in which part of divalent metal cations has been substituted by trivalent cations resulting in the positively charged layers. Negatively charged species formed by exchangeable anions and water molecules ensuring structural electroneutrality. The wide range of preparation methods and compositions makes it possible to obtain materials with specific properties. Currently there is intense interest in finding uses for these materials in catalysis and as adsorbents [1–5].

The present paper deals with the synthesis and the characterization of new iridium, platinum and ruthenium containing LDHs prepared by exchanging chloride anions in [ZnAlCl], [MgAlCl] and [CuAlCl] with $[IrCl_6]^{3-}$, $[PtCl_6]^{2-}$, and $[RuCl_6]^{3-}$ anions.

The choice of these anions as the complexes to be trapped in the interlayer domain results in a structural preservation during hydrolysis and in really interesting possibilities of these noble metals in catalysis [5–13].

These materials could be precursors to metallic or oxide nanoparticles with at least two metal elements as it appeared in the literature [14,15]. So, one aim could be the preparation of metallic particles on oxide support by using thermal treatment in order to replace impregnation method. Different new [ZnAl], [MgAl] and [CuAl] LDHs intercalated with iridium complex, co-intercalated with iridium and platinum complexes and co-intercalated with ruthenium and platinum complexes were prepared. They are hereafter noted [ZnAlIr]; [MgAlIr]; [CuAlIr]; [ZnAlIrPt]; [MgAlIrPt]; [ZnAlRuPt]; [MgAlRuPt]. The obtained results are compared with those from LDH containing platinum complexes [16].

2. Experimental section

2.1. Samples preparation

$[ZnAlCl]_{LDH}$, $[MgAlCl]_{LDH}$ and $[CuAlCl]_{LDH}$ with formulas $[Zn_2Al(OH)_6]Cl\cdot 2H_2O$, $[Mg_2Al(OH)_6]Cl\cdot 2H_2O$, $[Cu_2Al(OH)_6]Cl\cdot 2H_2O$ were used as precursors to be exchanged with $[MCl_6]^{n-}$ anions.

*Corresponding author. Laboratoire des Matriaux Inorganiques, University Clermont Ferrand, ESA CNRS 6002, 24, Avenue des Landais, 63177 Clermont Ferrand, France. Fax: +33-4-73-40-71-08.
E-mail address: marie.de_roy@univ-bpclermont.fr (M.E. De Roy).

0022-4596/$ - see front matter © 2004 Elsevier Inc. All rights reserved.
doi:10.1016/j.jssc.2004.03.048

2.1.1. Synthesis of precursors

The precursors were prepared by a co-precipitation method at controlled pH as described in the literature [16,17].

Mixed solutions of $ZnCl_2$ (Prolabo, 99%)—$AlCl_3 \cdot 6H_2O$ (Sigma, 99%), $MgCl_2 \cdot 6H_2O$ (Sigma, 98%)—$AlCl_3 \cdot 6H_2O$ and $CuCl_2 \cdot 2H_2O$ (Prolabo, 99%)—$AlCl_3 \cdot 6H_2O$ in the expected M^{II}/Al molar ratio having total cation concentration of 1 M were used. The pH was maintained during co-precipitation at 8.5, 9.5 and 5.5, respectively, by simultaneous addition of 1 M NaOH. Synthesis was performed at room temperature except for [MgAlCl] (65°C), under nitrogen atmosphere to prevent contamination by carbonate from atmospheric CO_2. Deionized decarbonated water was used throughout all the experiments.

2.1.2. Anionic exchange

The same method with few variations was used for exchange process with the three precursors. For example, this process is described hereafter for $[IrCl_6]^{3-}$ exchange. The first step consisted in adding precursors in aqueous solutions of K_3IrCl_6 (Aldrich 99%) containing higher ratio of the complexes than the anionic exchange capacity of the LDH, during various times (Table 1); the pH solution was near to 5.5. In the second step, the suspension was stirred in an autoclave and heated firstly at 50°C (autogeneous pressure 1 kbar) and secondly at 120°C (autogeneous pressure 2.4 kbar) during suitable times reported in Table 1.

Concerning co-intercalation, the same steps were used (Table 1); initial mixed anions solutions were K_3IrCl_6 (Aldrich 99%)/K_2PtCl_6 (Strem 99%) = 50/50 for [ZnAlIrPt] and [MgAlIrPt] and K_3RuCl_6 (Aldrich 99%)/K_2PtCl_6 (Strem 99%) = 80/20 for [ZnAlRuPt] and [MgAlRuPt].

Powdered products were recovered after cooling the autoclave by centrifugation, washed with deionized water three times and dried at 50°C for 12 h.

This way of hydrothermal synthesis was chosen because several attempts using the commonly described methods such as simple exchange did not permit the intercalation of complexes.

2.2. Characterization techniques and procedures

Powder X-ray diffraction patterns were recorded on a Siemens D 501 X-ray diffractometer using Cu$K\alpha$ radiation and fitted with a graphite-scattered beam monochromator. The samples as unoriented powder were scanned from $2\theta = 2°$ to 76° in steps of 0.08° with count time of 4 s at each point. Fourier transform infra red spectra were obtained with a Perkin Elmer 16PC spectrophotometer at a resolution of 2 cm^{-1} and averaging ten scans in the 400–4000 cm^{-1} region on pressed KBr pellets. Thermogravimetry was recorded on a Setaram TG DTA 92 analyzer at a rate of 5°C min^{-1} under air atmosphere. The nitrogen adsorption isotherms of the samples at liquid nitrogen temperature were recorded on a Coulter SA 100. Prior to isotherm measurements, samples were degazed for 500 min at the suitable temperature provided by TG analysis in order to remove the adsorbed and interlayer water. Pore distribution in all samples were calculated using the BJH model on the desorption mode. Element analyses were performed at the Vernaison Analysis Center of CNRS. Zn K-edge- and Ir L_{III}-edge-extended X-ray absorption fine structure studies (EXAFS) were performed at LURE (Orsay, France) using X-ray synchrotron radiation emitted by the DCI storage ring (1.85 GeV positrons, average intensity of 250 mA) at the D44 line. Data were collected at room temperature in transmission mode at the Zn K-edge (9.658 keV) and Ir L_{III}-edge (11.2152 keV). Three spectra were recorded for each sample. [ZnAlCl] and K_3IrCl_6 were taken as the reference materials; the theoretical functions from Mc Kale's tables were taken as the phase and amplitude [18]. The EXAFS signal treatments and refinements

Table 1
Synthesis parameters for exchanged samples

Exchanged precursor	First step reaction time (min)	Second step reaction time (min)	
		50°C	120°C
$[IrCl_6]^{3-}$ intercalation: molar excess of metal complex for exchange process = 3.2			
[Zn2AlCl]	80	410	70
[Mg2AlCl]	60	410	60
[Cu2AlCl]	50	410	60
$[IrCl_6]^{3-}$ and $[PtCl_6]^{2-}$ co-intercalation: molar excess of metal complex for exchange process = 3.2, $[IrCl_6]^{3-}/[PtCl_6]^{2-}$ = 50/50			
[Zn2AlCl]	90	410	100
[Mg2AlCl]	90	410	90
$[RuCl_6]^{3-}$ and $[PtCl_6]^{2-}$ co-intercalation: molar excess of metal complexes for exchange process = 3.5, $[RuCl_6]^{3-}/[PtCl_6]^{2-}$ = 80/20			
[Zn2AlCl]	20	410	100
[Mg2AlCl]	20	410	90

were performed with the program package developed by Michalowicz [19]. The commonly accepted fitting accuracy was about 0.02 Å for the distance and 10–20% for the number of neighbors. The module of the Fourier transform corresponded to the pseudo-radial distribution functions (pseudo RDF).

3. Results and discussion

3.1. Characterization of exchanged layered double hydroxides

3.1.1. Chemical and XRD analysis

For all compounds, the diffraction peaks are indexed using a hexagonal cell with rhombohedral symmetry (*R*-3*m*) where the *c* parameter corresponds to three times the interlamellar distance *d*(003) and the *a* parameter, which represents the average intermetallic distance, is calculated from the position of the *d*(110) peak. Cell parameters in precursors and in exchanged products are compared in Table 2. According to the patterns definition, they were refined using at least 10–12 peaks in each diffractograms.

The completeness of chloride exchange by the anionic complexes of noble metals was confirmed by chemical analysis and X-ray powder diffraction for $[IrCl_6]^{3-}$ and $\prod[PtCl_6]^{2-}$ anions.

Concerning [CuAlIr] compound, the XRD pattern was not sufficiently defined for cell parameter determination. For Ir and Pt containing samples, the increasing of *c* parameter corresponded to the presence of metal complex between the layers. On the contrary, we noted that [ZnAlRuPt] and [MgAlRuPt] cell parameters values are rather similar to those of precursors which will be discussed below.

For all the compounds, we observed an inverse of intensity for the two first (00*l*) peaks in exchanged products comparatively to the LDH chloride precursors (Fig. 1). This phenomenon appeared in previous works for LDHs containing heavy interlayer molecular species

Table 2
Cell-parameters and basal spacing (*d*) in an *R*-3*m* symmetry

Samples	*a* (nm)	*c* (nm)	*d* (nm)
[ZnAlCl]	0. 3089(1)	2.3715(7)	0.7905
[ZnAlPt][a]	0.3066(3)	3.0940(8)	1.0313
[ZnAlIr]	0.3068(5)	3.0920(6)	1.0306
[ZnAlIrPt]	0.3059(7)	3.0604(4)	1.0201
[ZnAlRuPt]	0.3072(6)	2.3724(1)	0.7908
[MgAlCl]	0.3073(9)	2.3860(5)	0.7953
[MgAlPt][a]	0.3067(4)	3.2103(1)	1.0701
[MgAlIr]	0.3046(4)	3.0536(2)	1.0178
[MgAlIrPt]	0.3031(7)	3.1020(2)	1.0341
[MgAlRuPt]	0.3047(4)	2.3283(2)	0.7761

[a] From Ref. [16].

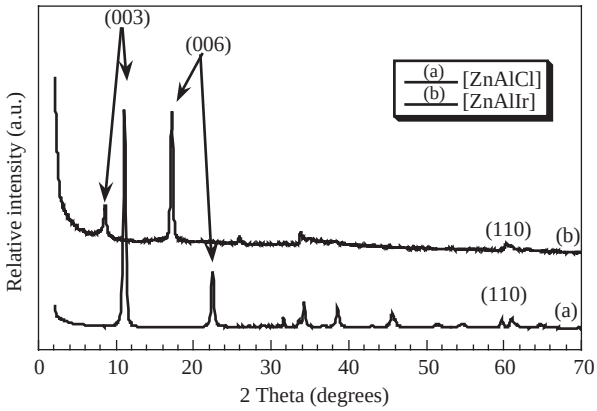

Fig. 1. XRD patterns of [ZnAlIr] and [ZnAlCl] compounds.

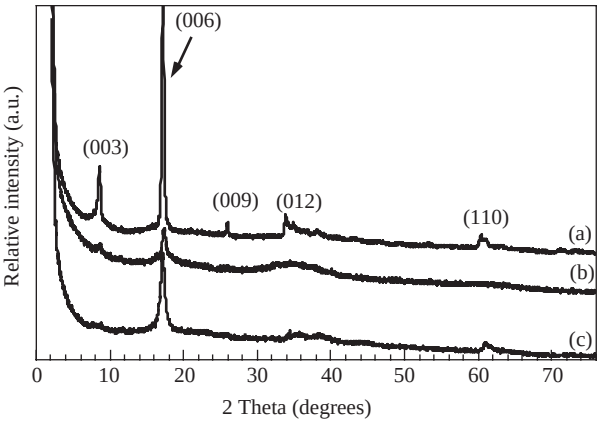

Fig. 2. XRD patterns of [ZnAlIr] (a), [CuAlIr] (b), and [MgAlIr] (c) compounds.

such as chromate or vanadate anions between [MgAl] layers, $[Al(C_2O_4)_3]^{3-}$ anions between [ZnAl] layers or hybrid hexa-chlorohydroxo-platinum anions between [ZnAl], [MgAl] and [CuAl] layers [20,21,16]. This has been attributed to the increase in electron density in the midplane of the interlayers due to the presence of the heavy metal, as explained in a previous work [16]. In this case, the XRD patterns showed an important intensity ratio between (003) and (006) diffraction lines, which could be linked to the high electronic density of the noble metal.

This observation clearly pointed out the presence of a heavy atom between the layers.

3.1.2. $[IrCl_6]^{3-}$ intercalated compounds

X-ray powder diffraction patterns of $[IrCl_6]^{3-}$ exchanged products are presented in Fig. 2. For [MgAl] and [CuAl] LDH compounds, we observed an important amorphous phase. However, there was no residue of crystallized LDH chloride precursors.

Chemical composition of obtained compounds are reported in Table 3. In all cases, chloride contents was lower than expected, while hydroxyl group content was

Table 3
Chemical compositon of exchanged LDHs

HDLs samples	M^{II}/M^{III}	Cl/Mc	Pt/Mc
[ZnAlCl]	1.98	—	—
[ZnAlIr]	1.80	3.45	—
[ZnAlIrPt]	1.91	2.40	0.62
[ZnAlRuPt]	1.83	1.08	0.35
[ZnAlPt][a]	1.51	3.2	—
[MgAlCl]	2.06	—	—
[MgAlIr]	1.72	2.5	—
[MgAlIrPt]	1.91	1.9	0.40
[MgAlRuPt]	1.80	1.02	0.36
[MgAlPt][a]	1.79	3.6	—
CuAlCl	2.04	—	—
CuAlIr	1.81	2.5	—
CuAlPt[a]	1.69	2.4	—

Mc: metal of intercalated complex.
[a] From Ref. [16].

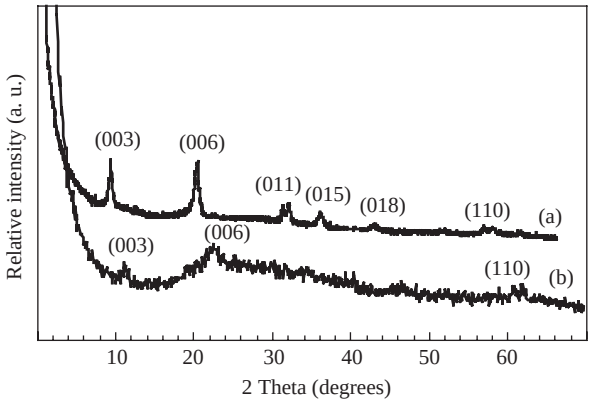

Fig. 3. XRD patterns of [ZnAlRuPt] (a) and [MgAlRuPt] (b) compounds.

higher. We obtained similar results in the study of the $[PtCl_6]^{2-}$ complex evolution during the exchange in LDH phases [16], which could be related to progressive and well known hydrolyzis of $[IrCl_6]^{3-}$ [22–24], $[RuCl_6]^{3-}$ [25] and $[PtCl_6]^{2-}$ [26–29].

After exchange, we noted a slight decrease in M^{II}/M^{III} molar ratio, which could be explained by partial dissolution of divalent layer-composing cations (Zn, Mg, Cu) according to the pH domains generally admitted for $[PtCl_6]^{2-}$, $[IrCl_6]^{3-}$ and $[RuCl_6]^{3-}$ stability ($2 \leqslant pH \leqslant 6$)) or by a restoration phenomenon owing to hydrothermal synthesis conditions. The existence of defective sheets has already been noted for tetracyanoquinodimethane [30], and $[RuCl_5H_2O]^{3-}$ [31] between [ZnAl] layers; it was also reported for the synthesis of pillared clays with Keggin heteropoly anions [32].

3.1.3. Co-intercalated compounds

Co-intercalated $[PtCl_6]^{2-}/[IrCl_6]^{3-}$ LDHs: For the two compounds, metal complexes appeared more hydrolyzed when they were co-intercalated compared to simple intercalation under the same conditions, and the initial ratio $[PtCl_6]^{2-}/[IrCl_6]^{3-}$ was modified during exchange process.

Co-intercalated $[PtCl_6]^{2-}/[RuCl_6]^{3-}$ LDHs: We observed that basal spacings were nearly the same as for precursors, but at the same time the intensities of the two first (00*l*) peaks were modified and an amorphous phase appeared (Fig. 3). Considering the basal spacing values, intercalation of complexes like $[MCl_{(6-x)}(OH)_x]^{k-}$ could not be considered.

Chemical analysis showed that, in spite of many washing cycles, ruthenium and platinum were part of the samples composition. A possible explanation could be the existence of Ru–Pt clusters as reported by Alerasool and Gonzalez [33,34] who observed such clusters on silica or alumina supports after the impregnation of H_2PtCl_6 and $RuCl_3$. It was proved that the clusters were negatively charged and pH dependent [35]. Diaz et al. [35] reported the existence of Pt–Ru clusters on alumina support with different molar ratios (3.0; 1.0 and 0.33), rather close to our values (0.35 and 0.36). According to the conclusions of Diaz et al., we suppose that some clusters could be formed during the synthesis from combinations between initial complexes and some non-metal elements coming from layers. These clusters could be bound on powder surface.

3.1.4. FT-IR characterization

For $[PtCl_6]^{2-}$, $[IrCl_6]^{3-}$, and $[RuCl_6]^{3-}$ anions, the literature [36] gives characteristic IR bands at frequencies lower than $400\,cm^{-1}$. So part of IR study was performed in CsI using diffuse reflectance method. However, only exploitable results were obtained for platinum complexes [16].

Furthermore, no information was available on mixed complexes such as $[IrCl_{(6-x)}(OH)_x]^{3-}$ or $[RuCl_{(6-x)}(OH)_x]^{3-}$. Concerning exchanged LDHs, their IR studies were performed between 4000 and $400\,cm^{-1}$. For Ir and Pt containing samples, IR spectra corresponded to compounds free of carbonate contamination. On the contrary, [MgAlRuPt] and [ZnAlRuPt] IR spectra showed some extra weak IR bands characteristic of carbonate species. As carbonate containing HDLs structure was not evidenced in XRD study, we think that carbonate species could be adsorbed on surface rather than intercalated between layers. This is particularly evidenced by the IR band around $1400\,cm^{-1}$ characteristic of adsorbed CO_3^{2-} species. Assigned bands are presented in Table 4.

3.1.5. X-ray absorption spectroscopy

X-ray absorption spectra were recorded at the Zn *K*-edge (9.658 keV) for [ZnAlCl] and [ZnAlIr] and at Ir L_{III}-edge (11.215 keV) for K_3IrCl_6 and [ZnAlIr]. Concerning co-intercalated LDHs, no exploitable results

Table 4
Infrared bands of intercalated compounds

Samples	υ (OH) (cm^{-1})	δ (H_2O) (cm^{-1})	υ_{M-O} (cm^{-1})	δ_{O-M-O} (cm^{-1})	$v1$ $(CO_3)^{2-}$ (cm^{-1})	$v3$ $(CO_3)^{2-}$ (cm^{-1}) (ads)	$v3+v4$ $(CO_3)^{2-}$ (cm^{-1})
[ZnAlPt][a]	3510	1623	600	430	—	—	—
[MgAlPt][a]	3450	1625	630	400	—	—	—
[CuAlPt][a]	3480	1623	590	440	—	—	—
[ZnAlIr]	3492	1623	608	410	—	—	—
[MgAlIr]	3482	1625	658	460	—	—	—
[CuAlIr]	3472	1623	588	450	—	—	—
[ZnAlIrPt]	3482	1633	658	410	—	—	—
[MgAlIrPt]	3460	1643	638	450	—	—	—
[ZnAlRuPt]	3430	1600	590	410	1010	1400	2380
[MgAlRuPt]	3430	1593	570	460	1005	1390	2380

[a] From Ref. [16].

Table 5
EXAFS results for Ir atom local environment (first coordination shell)

Sample	N_1	R_1(nm)	N_2	R_2 (nm)	$\sigma_1=\sigma_2$ (10^4 nm^2)	F
K_2PtCl_6[a]	6	0.231	0	-	5.94	7.92 10^{-3}
K_3IrCl_6	6	0.234	0	-	5.50	9.49 10^{-3}
[ZnAlPt][a]	2.73	0.199	3.27	0.232	5.94	8.53 10^{-3}
[ZnAlIr]	2.44	0.202	3.56	0.234	5.50	1.05 10^{-3}

σ_i: Debye–Waller factor; N_i: Effective coordination number; R_i: Interatomic distance between an atom and its neighbors; F: disagreement factor.
[a] From Ref. [16].

could be obtained with the Ir and Pt L_{III}-edge values, which are closely related (11.215 and 11.563 keV).

Concerning Zn environment in LDHs, the study at the Zn K-edge carried out on [ZnAlCl] and [ZnAlIr] showed that the two pseudo radial distribution functions were superimposed proving that local order around Zn cations in layers was preserved after exchange with iridium complex.

A strongly distorted and mixed environment appeared around iridium cation for the intercalated complex. Refinement parameters, obtained with only single scattering contribution, are reported in Table 5. Hexacoordinate environment was preserved but with mixed ligands. The Fourier transform representation, related to the first coordination shell in [ZnAlIr], showed a broader peak, in comparison to the reference compound K_3IrCl_6. We could not observe two separated peaks for the intercalated platinum complex but the best modelling results led to an Ir-mixed complex containing 2.44 (OH) ligands (Table 5).

Such results, already reported for intercalated platinum complexes [16], point out a partial hydrolysis of metal halocomplexes residing between LDHs layers. These results are in agreement with the chemical composition data (Table 3).

3.1.6. TG analysis

Thermal decompositions of [ZnAlIr], [MgAlIr], [CuAlIr] (Fig. 4), [ZnAlIrPt], and [MgAlIrPt] were

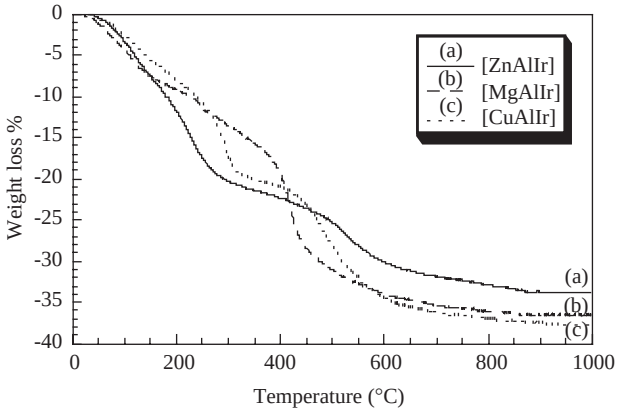

Fig. 4. TG analysis for [ZnAlIr] (a), [MgAlIr] (b), and [CuAlIr] (c) compounds.

rather similar and in good agreement with chemical compositions data. The desorption of adsorbed water was complete around 120°C while the desorption of structural water molecules occurs at higher temperatures and was complete at 230–300°C. The next step in weight loss was due to dehydroxilation of LDHs and release of chloride anions coming from the intercalated metallic complex. These two decompositions were not separated but one can here assume that the dehydroxylation occurred at a lower temperature than that of intercalated anion decomposition [37], which was complete around 820–880°C. For [MgAl] phases, even if the dehydroxylation occurred at a lower temperature than for [ZnAl] and [CuAl] phases, the final decomposition was observed at the same temperature. [ZnAl] phases appeared more hydrated than [MgAl] and [CuAl] ones.

Concerning [ZnAlRuPt] and [MgAlRuPt] a different behavior was observed. A continuous loss of weight appeared from the beginning of heating to 800°C. The measured weight loss at 800°C was lower than that measured for chloride precursors (28% and 32% for [ZnAlRuPt] and [MgAlRuPt], respectively). The lower proportion of volatile species in Ru–Pt co intercalated

compounds could be related to the existence of metallic clusters on LDHs surface. Otherwise, the difference in weight loss between [MgAlRuPt] and [ZnAlRuPt] was in good agreement with element analysis which showed that Mg-containing sample was more hydrated.

3.2. Characterization of layered double hydroxides upon thermal treatment

3.2.1. XRD characterization

Results of XRD analysis of samples heated to 950°C are given in Table 6. The XRD patterns of [ZnAlIr] are given in Fig. 5 as an example.

As temperature increased, the similar thermal behavior was observed for all the phases, the first stage corresponding to the amorphization of LDHs while the second stage being characterized by the formation of metal oxide and mixed oxide spinel. Metallic particles were evidenced on some calcined phase X-ray patterns by the Pt X-ray peaks for varying temperatures according to HDLs composition (Table 6).

For [ZnAlRuPt] and [MgAlRuPt], a different behavior was observed. Firstly the amorphization of LDH material and the formation of ruthenium oxide was observed. Secondly, mixed metal oxide appeared at a higher temperature than for the other samples. The crystallinity of ruthenium oxide decreased from 600°C unlike the oxide and mixed oxide from the layers. Metallic platinum appeared at lower temperatures for [MgAl] phase than for [ZnAl] phase, as it was shown for samples containing platinum complex [16]. The formation of metallic ruthenium for [MgAlRuPt] at 900°C, contrary to [ZnAlRuPt], was a notable fact. It showed the importance of layer composition during the decomposition and basic sites from magnesium seemed making the reduction easier. An important fact for this compound was the simultaneous presence of ruthenium and platinum metals on oxide support. In comparison, Inacio et al., reported that $[RuCl_5(H_2O)]^{3-}$ intercalated into LDH could not be reduced even with hydrogen or by electrochemical process [31]. The easier ruthenium reduction process in [MgAlRuPt] relative to intercalated $[RuCl_5H_2O]^{3-}$ could confirm that ruthenium species were not trapped between LDHs layers.

Table 6
Oxides and metals obtained after calcination and identified by XRD

LDHs	Temperature of crystallization of oxides and metals (°C)				
$[M^{II}M^{III}Ir]$	$[M^{II}O]$	$[M^{II}M^{III}_2O_4]$	IrO_2		
[ZnAlIr]	500	600	500		
[MgAlIr]	400	—	700		
[CuAlIr]	500	700	700		
$[M^{II}M^{III}IrPt]$	$[M^{II}O]$	$[M^{II}M^{III}_2O_4]$	IrO_2	Pt	
[ZnAlIrPt]	600	600	600	900	
[MgAlIrPt]	420	820	620	620	
$[M^{II}M^{III}RuPt]$	$[M^{II}O]$	$[M^{II}M^{III}_2O_4]$	RuO_2	Ru	Pt
[ZnAlRuPt]	740	800	400	—	900
[MgAlRuPt]	600	740	400	900	600

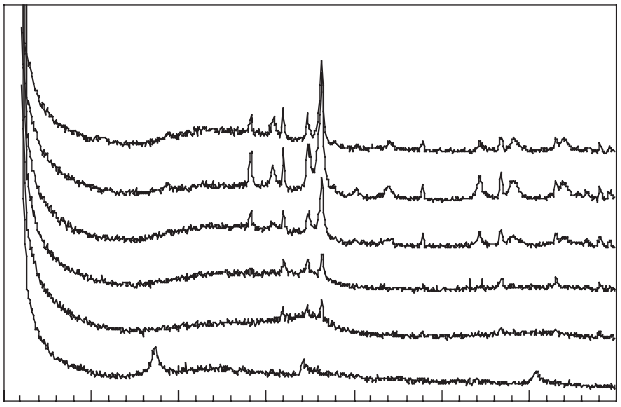

Fig. 5. XRD patterns of [ZnAlIr] LDH calcined at various temperatures: (a) 200°C, (b) 400°C, (c) 500°C, (d) 600°C, (e) 700°C, and (f) 800°C.

3.2.2. N_2 volumetric and size measurements

Synthetic LDH compounds are widely used as precursors of mixed oxide catalysts whose surface area is of importance [38]. So we carried out a systematic analysis of the nitrogen adsorption–desorption processes of the intercalated LDHs. The N_2 adsorption-desorption curves for non-calcined compounds were typical of mesoporous materials demonstrating isotherms of IV type in Brunauer, Deming and Teller classification [39–40]. A similar behavior was earlier described for LDH reference materials such as [ZnAl] and [MgAl] containing chloride, carbonate [38] or platinum complexes anions [16].

At 25°C, the BET surface area values of exchanged LDHs were about those of chloride precursor values (25, 44 and $14\,m^2\,g^{-1}$ for [ZnAlCl], [MgAlCl] and [CuAlCl]) except for [MgAlRuPt] and [ZnAlRuPt] (Table 7).

The BET values of ruthenium containing LDHs could be explained by metallic cluster lying on powder surface.

At 400°C, contrary to [MgAl] phases, [ZnAl] and [CuAl] materials showed decrease or no significant variation of BET surface area values upon thermal treatment, but mesoporous structure was preserved. A rapid dehydration followed by a rapid crystallization of metal oxide was given as an explanation for these phenomena [41].

For compounds intercalated by only platinum or iridium complexes, significant BET surface area values appeared with a maximum at about 500–600°C.

The difference in surface areas between [MgAl]- and [ZnAl]-calcined materials appeared to be due to better crystallization of oxides, obtained from [ZnAl]

Table 7
Specific surface area for intercalated and calcined phases

Thermal treatment temperature (°C)	BET surface area $m^2 g^{-1}$ and C parameter[a]											
	25		400		490		620		820		890	
Compounds	S_{BET}	C	S_{BET}	C	S_{BET}	C	S_{BET}	C	S_{BET}	C	S_{BET}	C
[ZnAlPt][b]	40.6	53	32.5	55	68.8	68					16.9	101
[MgAlPt][b]	35.8	105	83	75	87.9	68	107.2	102	91.4	103	86.0	59
[CuAlPt][b]	18.2	67	15.2	70								
[ZnAlIr]	15.7	113	30.9	75	65.5	70	48.5	101				
[MgAlIr]	35.9	114			90.1	76	111.8	108	94.9	123		
[CuAlIr]	18.8	78	17.1	82								
[ZnAlRuPt]	85.2	102	73.8	108			45.7	105				
[MgAlRuPt]	166.2	103	130.3	112			92.9	113	101.9	125		
[ZnAlIrPt]	38.8	105	29.8	58								
[MgAlIrPt]	59.2	103	78.2	124			73.2	143	74	111		

[a] C is a characteristic physical constant of gas–solid studied system depending on condensation heat q as: $C = \exp((q_1 - q_L)/RT)$.
[b] Data at 25°C and 400°C from Ref. [16].

compounds in this temperature range. For [MgAlPt], [MgAlIr], and [MgAlIrPt], BET surface area values were almost constant within a wide temperature range.

It is noteworthy that calcined [MgAlRuPt] and [ZnAlRuPt] presented the same behavior as other calcined samples even if their BET surface area values were higher before thermal treatment.

At 25°C, BJH measurements of the pores size revealed a mesoporous structure (65–90 pore% by volume) for intercalated LDHs.

3.3. Layout of intercalated complexes between LDHs layers

According to XRD and EXAFS results, we tried to model the layout of mixed iridium complex between LDHs layers. The structural model used in order to obtain the free interlamellar space (d_{free}) was related to the equation $d_{free} = d_{obs} - (T_{Layer} + 2L_H)$.

- T_{Layer} represents the thickness of the layer consisting in $[MO_6]$ octahedra that is around 0.20 nm [42,43].
- L_H represents the hydrogen bond length between layers and anionic species that is around 0.27 nm [44].

Considering the values of d_{obs} for Ir-intercalated compounds (Table 2), the only possible orientation is that pseudo-C_3-axis of pseudo-octahedral anionic complexes were perpendicular to the brucite-like layers and aligned along the z-axis (Scheme 1 (A)). This behavior is partially different from that observed for platinum complex intercalated into LDH [16]. Indeed, for [MgAlPt] it was reported that the effective C_2-axis of the pseudo-octahedral anion was perpendicular to the brucite-like layers and aligned along the z-axis (Scheme 1 (B)).

It seems that the arrangement of complexes was not only influenced by the layer's basicity but also by the Cl/Mc ratio value (Table 3). Concerning [ZnAl] or [CuAl] layers, there was no observable major variation of basal spacing for different Cl/Mc values, and therefore we think that basicity was a determining parameter for complexes arrangement.

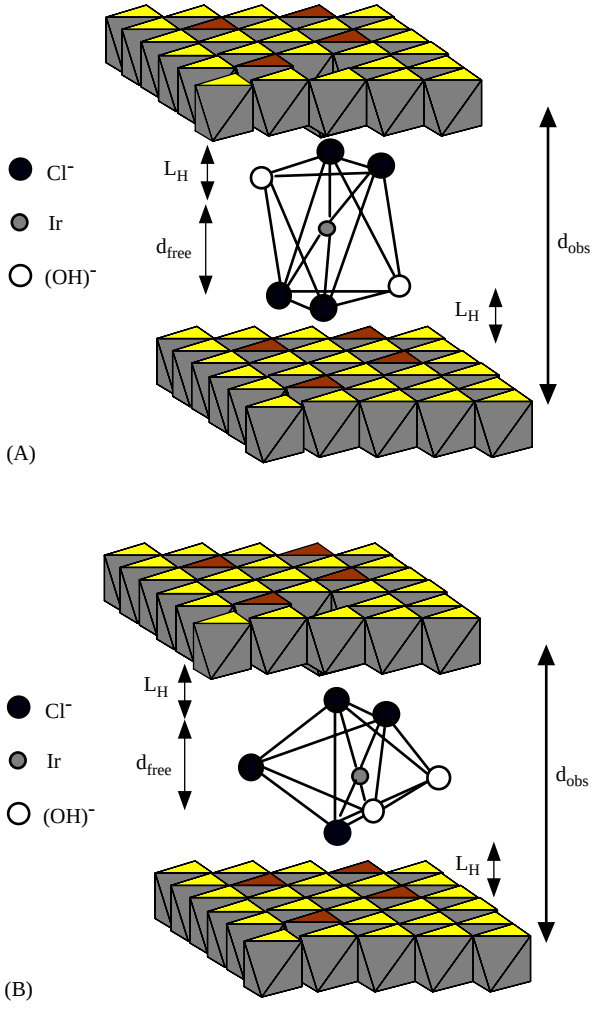

Scheme 1. Proposed layout of metallic complexes between layers: (A) for [ZnAlIr]; (B) for [MgAlPt].

4. Conclusion

Intercalation of chloride LDHs with noble metal complexes was successfully achieved and confirmed by XRD and FTIR data. A total anion exchange occurred without carbonate impurities for Ir and Pt complexes. However, element analysis and EXAFS study revealed a complex behavior of intercalated complexes with loss of Cl^- ligands due to simultaneous occurring of hydrolysis. Composition of layers seemed to influence the hydrolysis rate of the intercalated complexes. The preserved amount of Cl^- controlled the position of complexes between [MgAl] layers and basal spacing. These data allowed to model the layout of noble metal complex between layers in [MgAlIr]. For Ru–Pt containing LDHs, the most consistent hypothesis was the formation of clusters lying on the surface of a mixture of non-exchanged chloride precursors and an amorphous phase formed during hydrothermal treatment. However, at this time, even if Ru and Pt species presence was evidenced, we have no experimental proofs of such clusters existence. High specific surface areas, obtained after thermal treatment of LDHs and simultaneous formation of metallic particles of platinum and ruthenium on mixed oxide supports, were experimentally found for some of the studied compounds.

Acknowledgments

We thank ENSCCF for BET facilities and the LURE, Mr. A. de Roy, and Mr. F. Leroux for EXAFS measurements. Mrs. P. Ceysset as translator for helpful discussions.

References

[1] S. Miyata, Clays Clay Miner. 28 (1980) 50.
[2] A. de Roy, C. Forano, K. el Malki, J.P. Besse, in: Ocelli and Robson (Eds.), Anionic Clays: Trends in Pillaring Chemistry, Vol. II, Van Nostrand Reinhold New York, 1992, p. 108 (Chapter 7).
[3] A. Vaccari, Appl. Clay Sci. 14 (1999) 161.
[4] I. Rousselot, C. Taviot-Guého, J.P. Besse, Int. J. Inorg. Mater. 1 (1999) 165.
[5] L. Basini, D. Sanfilippo, J. Catal. 157 (1995) 162.
[6] G. Szollosi, I. Kun, A. Mastalir, M. Bartok, I. Dekany, Solid State Ionics 141–142 (2001) 273.
[7] C. Micheaud-Especel, D. Bazin, M. Guérin, P. Marécot, J. Barbier, React. Kinet. Catal. Lett. 69 (2000) 209.
[8] E. Guillon, J. Lynch, D. Uzio, B. Didillon, Catal. Today 65 (2001) 201.
[9] Z. Vit, J. Cinibulk, React. Kinet. Catal. Lett. 72 (2001) 189.
[10] E. Auer, M. Gross, P. Panster, K. Takemoto, Catal. Today 65 (2001) 31.
[11] K. Nakagawa, K. Anzai, N. Matsui, N. Ikenaga, T. Suzuki, Y. Teng, T. Kobayashi, M. Haruta, Catal. Lett. 51 (1998) 163.
[12] U.L. Portugal Jr., C.M.P. Marques, E.C.C. Araujo, E.V. Morales, M.V. Giotto, J.M.C. Bueno, Appl. Catal. A: Gen. 193 (2000) 173.
[13] E. Dietzsch, P. Claus, D. Honicke, Topics Catal. 10 (2000) 99.
[14] M. Freemantle, Chem. Eng. News 12 (1998) 40.
[15] R.V. Malyala, C.V. Rode, M. Arai, S.G. Hedge, R.V. Chaudhari, Appl. Catal. A: Gen. 193 (2000) 71.
[16] P. Beaudot, M.E. de Roy, J.P. Besse, J. Solid State Chem. 161 (2001) 332.
[17] S. Miyata, Clays Clay Miner. 31 (1983) 305.
[18] A.G. Mac Kale, B.W. Veal, A.P. Paulikas, S.K. Chan, J. Knapp, J. Am. Chem. Soc. 110 (1988) 3763.
[19] A. Mickalowicz, Programs available on the web site of LURE; http://www.lure.fr
[20] F. Malherbe, Ph.D. Thesis, Blaise Pascal University, France, 1997.
[21] V. Prévot, C. Forano, J.P. Besse, J. Solid State Chem. 153 (2000) 301.
[22] I.A. Paulsen, C.S. Garner, J. Am. Chem. Soc. 84 (1962) 2032.
[23] A.J.P. Domingos, A.M.T.S. Domingos, J.M.J. Peixoto Cabral, Inor. Nucl. Chem. 31 (1969) 2563.
[24] M.-L. Hung, M.L. McKee, D.M. Stanbury, Inorg. Chem. 33 (1994) 5108.
[25] E.A. Seddon, K.R. Seddon, in: R.J.H. Clark (Ed.), The Chemistry of Ruthenium, Elsevier, Amsterdam, 1984.
[26] P. Pascal, Nouveau traité de chimie minérale, Masson et Cie editor 19, 1958, p. 750.
[27] C. Carr, P.L. Goggin, R.J. Goodfellow, Inor. Chim. Acta 81 (1984) 25.
[28] P. Erlhöfer, W. Preetz, Z. Naturforsch. 44b (1989) 619.
[29] W. Preetz, G. Rimkus, Z. Naturforsch 37b (1982) 579.
[30] S. Bonnet, C. Forano, J.P. Besse, Mater. Res. Bull. 33 (1998) 783.
[31] J. Inacio, C. Taviot-Guého, S. Morlat-Thérias, M.E. de Roy, J.P. Besse, J. Mater. Chem. 11 (2001) 640.
[32] J. Wang, Y. Tian, R.C. Wang, A. Clearfield, Chem. Mater. 4 (1992) 1276.
[33] S. Alerasool, D. Boecker, B. Rejai, R.D. Gonzalez, G. Del Angel, M. Azomosa, R. Gomez, Langmuir 4 (1988) 1083.
[34] S. Alerasool, R.D. Gonzalez, J. Catal. 124 (1990) 204.
[35] G. Diaz, F. Garin, G. Maire, S. Alerassool, R.D. Gonzalez, Appl. Catal. A: Gen. 124 (1995) 33.
[36] K. Nakamoto, Infrared and Raman Spectra of Inorganic and Coordination Compounds, Wiley, New York, 1997.
[37] A. de Roy, A.M. Vernay, J.P. Besse, G. Thomas, Anulisis 16 (7) (1988) 409.
[38] A. Vaccari (Ed.), Synthesis and Applications of Anionic Clays, Elsevier, Amsterdam, 1995.
[39] S. Brunnauer, L.S. Deming, W.S. Deming, E. Teller, J. Am. Chem. Soc. 62 (1940) 1723.
[40] F. Malherbe, C. Forano, J.P. Besse, Micropor. Mater. 10 (1997) 67.
[41] V. Prévot, C. Forano, J.P. Besse, Inorg. Chem. 37 (1998) 4293.
[42] S. Bonnet, C. Forano, A. de Roy, J.P. Besse, P. Maillard, M. Momenteau, Chem. Mater. 8 (1996) 952.
[43] A. Ennadi, M. Khaldi, A. de Roy, J.P. Besse, Mol. Cryst. Liq. Cryst. 244 (1994) 373.
[44] M. Meyn, K. Beneke, G. Lagaly, Inog. Chem. 32 (1993) 1209.